Chapter 4: Results and Discussion

4.1. Chemistry

4.1.1. Conversion of piperine into piperic acid and synthesis of novel PA derivatives

The process for the development of **PA**, derivatives has been depicted in schemes 1 and 2. First, **PA (2a)** was synthesized from piperine **(1a)** in the presence of methanolic potassium hydroxide, followed by the neutralization of the reaction mixture by hydrochloric acid as reported in the literature(28).

4.1.2. Chemistry involved in the synthesis of the first series of compounds

A series of the substituted 2-amino-N-phenyl acetamides (**6a-6n**), from substituted 2-chloro-N-phenyl acetamides (**3a-3n**) was developed as shown in **Fig. 2B**, following our earlier publications (14). The commercially available substituted anilines **2a-2n**, went through a mechanism of "nucleophilic acyl substitution" with chloroacetylchloride in DCM and K_2CO_3 as base to give corresponding substituted 2-chloro-N-phenyl acetamides **3a-3n**. These were further refluxed at 60°C in the excess of NH_3 to produce substituted 2-amino-N-phenyl acetamides **4a-4n** in 60-70 % yields without purification. At the end, the compounds **6a-6n** were synthesized using standard amide coupling reaction of the substituted 2-amino-N-phenyl acetamides with **PA** resulting in a good yield (60-70 %). Synthesized derivatives were confirmed with the help of ^{1}H and ^{13}CNMR, and HRMS (Supporting Information).

Scheme 1. Synthesis of piperic acid from piperine

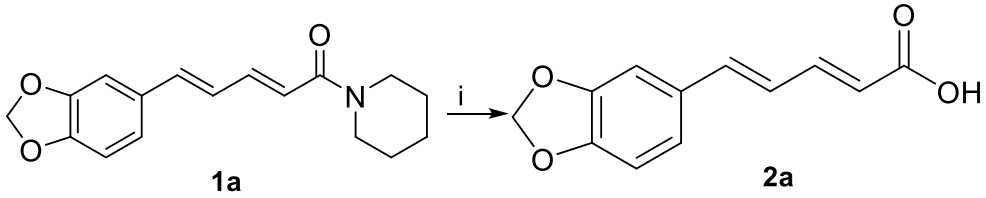

Reagents and conditions: (i) CH_3OH, KOH, 65 °C, 48 hr, neutralization by HCl, 65-70 %.

Scheme 2. Synthesis of piperic acid-acetamides derivatives **6a-6n**

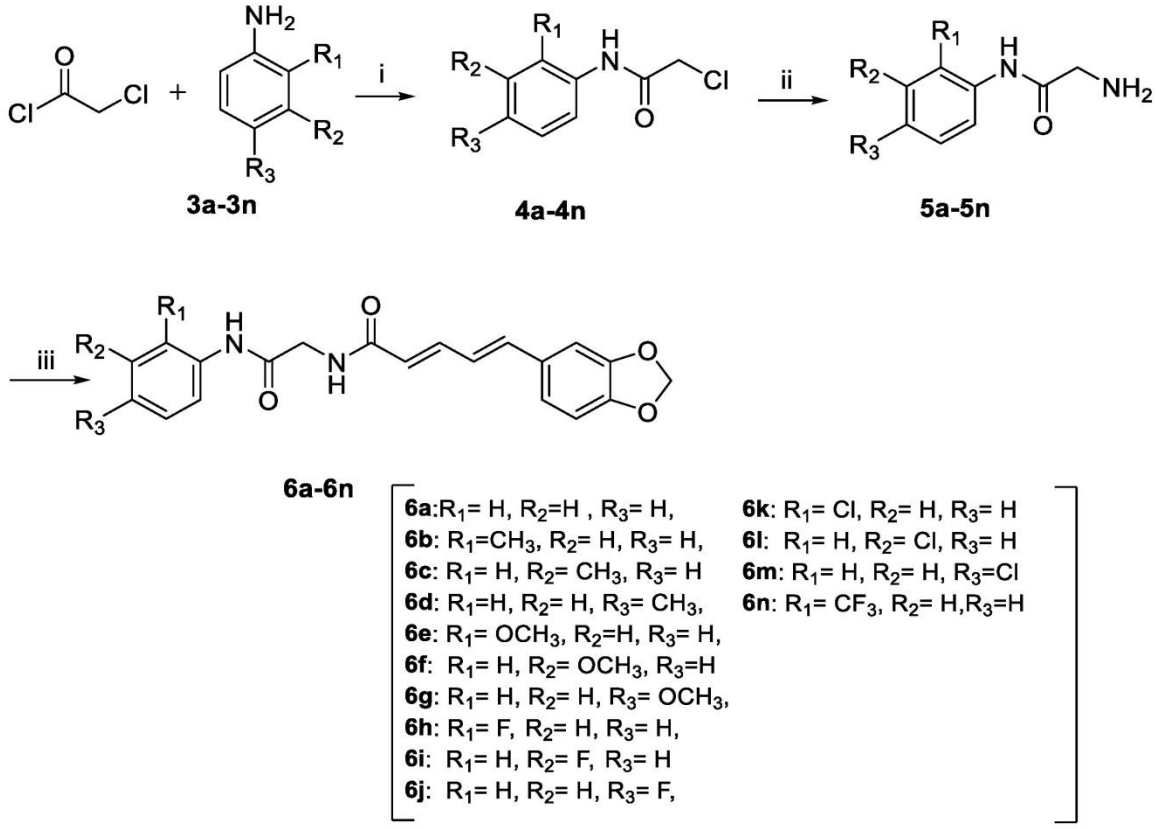

Reagents and conditions: (i) K_2CO_3, DCM, 0°C, 2 hr, 60-70 %; (ii) Excess NH_3, 60 °C, 6 hr, 50-60 %; (iii) Piperic acid, EDCI, HOBt, DIPEA, THF, rt, 10-12 hr, 60-70 %

4.2. Biological evaluation of the first series of compounds

4.2.1. Cholinesterase inhibition studies

Given the fact that ACh (acetylcholine) and BCh (butyrylcholine) play a key role in memory loss and cognitive decline in AD, therefore, by measuring the inhibitory potential of AChE and BChE will indirectly indicate the potential of the molecules maintain the levels of Ach and BCh. We evaluated the inhibitory potential of the synthesized compounds against AChE and BChE using the Ellman spectroscopic method and our publications (14, 16). The effectiveness of the inhibitors was determined by their IC_{50},

which is the effective concentration of the drug that blocks 50 % of the ChEs enzyme. The marketed drug DPZ was used as reference drug used in this study (14).

The pharmacophore **PA** was the starting template for designing the potent ChE inhibitors. We started our research with the simple phenyl-bearing compound **6a**. Therefore, compound **6a** was designed and synthesized. As evident from Table 1 that **6a** could effectively inhibit AChE (% inhibition 46.06 ± 0.98 and 34.42 ± 0.12 for AChE and BChE, respectively) over **PA** (7.14 ± 0.98 and 5.87 ± 0.76 for AChE and BChE, respectively) which strongly suggests the favourable interaction of aromatic feature for the enzyme inhibition property. We further introduced methyl group onto the phenyl ring of our lead molecule **6a** to explore the role of small electron donating group (EDG) *o*-CH_3, *m*-$CH_3$and *p*-CH_3, which led to the generation of compounds **6b**-**6d**. Interestingly, **6b** bearing *o*-CH_3 on the phenyl ring showed maximum AChE and BChE inhibition over **6c** and **6d** (% inhibition, 53.27 ± 0.23, 37.15 ± 0.35 and 34.99 ± 0.38 for **6b-d**, respectively). We further introduced various electron-donating groups (*o*-CH_3, *m*-OCH_3, and *p*-OCH_3) on the phenyl ring, which leads to generation of compounds **6e**-**6g**. Interestingly, compounds **6g** showed the maximum inhibition for ChE among all EDG analogous (% inhibition (AChE) 39.76 ± 0.76, 43.50 ± 0.22, and 53.46 ± 0.34 for **6e-g**, respectively; % inhibition (BChE) 17.54 ± 0.22, 10.09 ± 0.82, 21.6 ± 0.55, for **6e-g**, respectively). After optimizing the electron-donating groups, we further introduced various electron-withdrawing groups (EWG) on the the phenyl ring to measure the role of substituents *o*-F, *m*-F, *p*-F, *o*-Cl, *m*-Cl, *p*-Cl, and *o*-CF_3 which led to the generation of compounds **6h**-**6n**. In the enzyme inhibition study, compounds **6j** and **6k** bearing *p*-F and *o*-Cl on the phenyl ring showed maximum inhibition for AChE among all EWG analogs (% inhibition (AChE) 48.68 ± 0.54, 56.39 ± 0.87, 66.72 ± 0.15, 58.40 ± 0.22, 55.99 ± 0.65, 48.09 ± 0.77, 58.46 ± 0.99; for **6h-n**, respectively; % inhibition (BChE) 17.30 ±

0.26, 19.30 ± 0.67, 28.19 ± 0.20, 20.90 ± 0.19, 2.13 ± 0.54, 13.67 ± 0.54, 19.90 ± 0.33 for **6h-n**, respectively). In the present study, we built up a SAR on the basis of various substitutions connected to phenyl ring (**Fig. 3**). Among the developed molecules, **6j** with a small electron withdrawing group was found to be the most potent against AChE.

Table 1.1. AChE and equine BChE inhibition studies

Compound	**R**	***h*AChE % inhibition / IC_{50}[a] (μM)**	***eq*BChE % inhibition / IC_{50} (μM)**
6a	Hydrogen	46.06 ± 0.98	34.42 ± 0.12
6b	2-methyl	53.27 ± 0.23	14.12 ± 0.66
6c	3-methyl	37.15 ± 0.35	11.33 ± 0.49
6d	3-methyl	34.99 ± 0.38	24.39 ± 0.11
6e	2-methoxy	39.76 ± 0.76	17.54 ± 0.22
6f	3-methoxy	43.50 ± 0.22	10.09 ± 0.82
6g	4-methoxy	53.46 ± 0.34	21.6 ± 0.55
6h	2-fluoro	48.68 ± 0.54	17.30 ± 0.26
6i	3-fluoro	56.39 ± 0.87	19.30 ± 0.67
6j	4-fluoro	2.13 ± 0.015μM	28.19 ± 0.20
6k	2-chloro	58.40 ± 0.22	20.90 ± 0.19
6l	3-chloro	55.99 ± 0.65	2.13 ± 0.54
6m	4-chloro	48.09 ± 0.77	13.67 ± 0.54
6n	2-trifluoromethyl	58.46 ± 0.99	19.90 ± 0.33
PA	----	7.14 ± 0.98	5.87 ± 0.76
DPZ	----	0.06 ± 0.01	2.16 ± 0.19

[a]IC_{50}: measure of the 50 % effectiveness of a drug inhibition concentration (mean ± SD of two different assays).

[b]%: effectiveness of a drug inhibition at 20 μM of inhibitor

[d]**PA**(acid) = negative control in an experiment for validation

[e]**DPZ** (donepezil) = reference compound for validation of the experiment

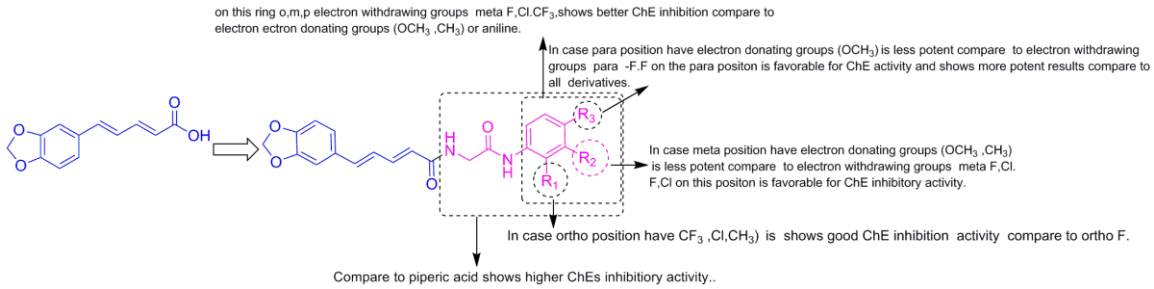

Figure. 4.1. Structural optimization and SAR with **PA** derivatives

4.2.2. The enzyme kinetics studies of 6j on AChE inhibition

The mechanism of AChE inhibition by compound **6j** was studied using human AChE (hAChE). The impact of compound **6j** on human acetylcholinesterase (hAChE) was investigated using a study that plotted velocity [V] against substrate [S] concentrations in the presence of various amounts of **6j** (26, 13, and 6.5 µM) and five different substrate [S] concentrations (0.5, 1.0, 1.5, 2.0, and 2.5 µM). The results, shown in **Fig. 4.2**, indicated that **6j** demonstrated mixed inhibition of hAChE as revealed by the Lineweaver-Burk reciprocal plots. (**Fig. 4.2**) (14).

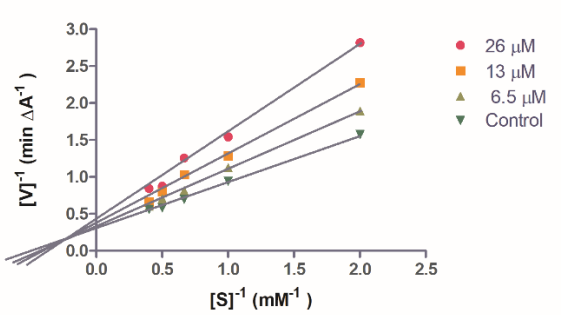

Figure. 4.2. Graphical representation of Lineweaver reciprocal plot depicting *h*AChE inhibition over a different concentration of the substrate; [**A**] *h*AChE inhibition by **6j.**

4.2.3. Propidium iodide displacement assay

In this experiment, the binding affinity of a newly developed molecule towards the PAS site of hAChE was evaluated using propidium iodide as a PAS-specific ligand. A drop in fluorescence intensity of propidium iodide was observed when propidium was pushed away from the PAS by the lead compound **6j**. The results presented in **Table 2** indicate

that the test molecule **6j** has a greater ability to displace propidium iodide (11.4 % at 50 µM) compared to **PA** (5.67 % at 50 µM). Additionally, DPZ showed a significant displacement of 30.88 % at 50 µM. These results provide insight into the binding affinity of the test molecule towards the PAS of hAChE(14, 16).

Table 1.2. Inhibition of the PAS by compound 6j

Compound	5 μM (%)	10 μM (%)	20 μM (%)	50 μM (%)
6j	1.23 ± 0.06	4.38 ± 0.31	6.45 ± 0.36	11.04 ± 0.27
PA	0.67 ± 0.26	1.56 ± 0.08	3.56 ± 0.06	5.67 ± 0.06
DPZ	10.56 ± 0.12	12.75 ± 0.34	22.65 ± 0.17	29.88 ± 0.31

[a]The results show the average value ± standard error of the mean, obtained from two separate experiments performed with three replicates each. DPZ = Donepezil

4.2.4. Evaluation of antioxidant activity by DPPH assay

The literature makes it clear that OS is crucial for AD development. As a result, inhibiting ChEs along with reducing oxidative stress would be a more successful strategy for treating AD (29) . The DPPH radical is a stable, nitrogen-centered free radical with an unpaired electron that is treated with the different concentrations of the molecule, **6e, 6i, 6j, 6k,** and **PA**. DPPH assay is a simple and most convenient *in vitro* method used to screen antioxidant candidates. We selected the most potent compounds **6e**, **6i**, **6j**, and **6k**, to evaluate their antioxidant capacity. The percentage radical scavenging activity values of **6e, 6i, 6j, 6k,** and **PA** were found to be 5.32±1.13, 15.23±1.13, 35.41 ±1.09, 23.94 ± 1.22 and 2.43 ±1.65% at 20 μM, respectively. As depicted in **Table 1.3**, compounds **6j,** and **6k** could significantly scavenge free radicals. On the other hand, **PA** displayed lower antioxidant activity than that of compounds **6j** and **6k** (14, 16, 30).

Table 1.3. Percent radical scavenging activity of compounds **6e, 6i, 6j and PA**

Compound	(%) Radical Scavenging activity [a]
6e	05.32 ± 1.13
6i	15.23 ± 1.13
6j	35.41 ± 1.09
6k	23.94 ± 1.22
[b]**PA**	02.43 ± 1.65

[a]The % Radical scavenging data expressed at 20 μM concentration; means ± SD of two independent experiment

[b]**PA** (Piperic acid) = used as a negative control to compare the experimental data

4.2.5. Metal chelation study

Studies have demonstrated that deficiencies or excesses of biometals in brain including, iron (Fe) and copper (Cu) may contribute to the onset of AD (12, 31). So, we performed metal chelation study of potent ChE inhibitor **6j** with $FeCl_3$ in order to understand their interaction with Fe (III) species. We recorded the absorbance spectrum of **6j** alone and **6j**in the presence of FeCl3 using a UV spectrophotometer over a range of 200-700 nm. As shown in **Fig. 4.3**, upon incubation with 1 equivalent of $FeCl_3$ with **6j**, neither absorption intensity enhancement nor any additional peaks were observed throughout the spectral range. The result suggests that the compound 6j did not effectively chelate the transition metal $FeCl_3$(14).

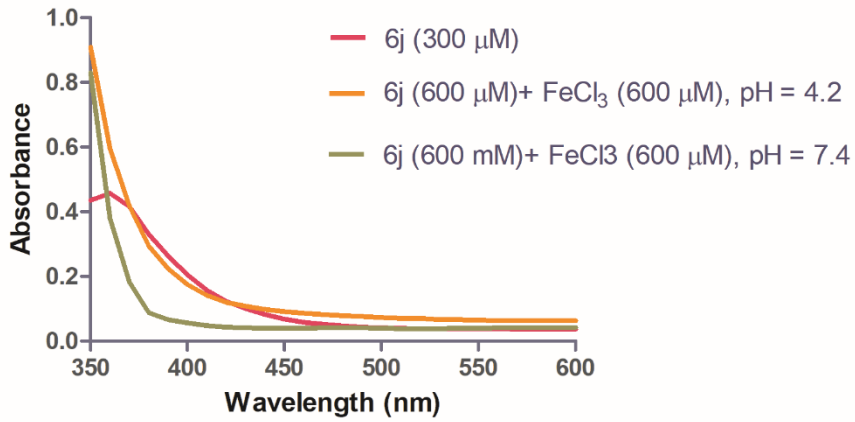

Figure. 4.3. UV-visible spectroscopic scanning of a solution containing 300 µM of **6j** alone in methanol and in combination with 600 µM of $FeCl_3$ at pH levels of 4.2 and 7.4, covering the range of 350-600 nM

4.2.6. Molecular modelling studies

4.2.6.1. Molecular docking

To explore the molecular interactions between the compounds and the AChE protein (PDB ID: **4EY7**), molecular docking approach was employed using Auto Dock software (20). The best docking poses of the compounds **6e** and **6j** along with reference compound DPZ are presented in **Fig. 4.4**. It was observed that the compounds bound at the same catalytic site after docking with the binding energy of -11.08 kcal/mol (**DPZ**), -10.11 kcal/mol (**6e**) and -9.79 kcal/mol (**6j**). Intriguingly, **6e** formed four conventional hydrogen bonds and one carbon-hydrogen bond with Tyr124, Phe295, Arg296, Tyr341 and Ser293 which is contrary to our enzyme inhibition studies. In addition, hydrophobic interaction and halogen bonds were also formed with Trp286, Val294, Phe338, Gln71, Asn87 and Trp86. In the case of compound **6j**, four conventional hydrogen bonds were formed with Ser293, Phe295, Arg296 and Tyr34. Besides these, three hydrophobic interactions and one halogen bond were also observed with Trp86, Tyr337, Phe338 and Asp74. However, the reference compound **DPZ** formed only one conventional hydrogen bond and two carbon-hydrogen bonds with Phe295, Tyr72 and Ser293 along with five hydrophobic interactions with residues Trp86, Trp286, Phe338, Tyr341 and His447. The **6e** and **6j** showed good binding affinity towards the AChE protein due to the formation of multiple hydrogen bonds and hydrophobic interactions, however, the binding energy for both the compounds were observed to be comparable with that of **DPZ**.

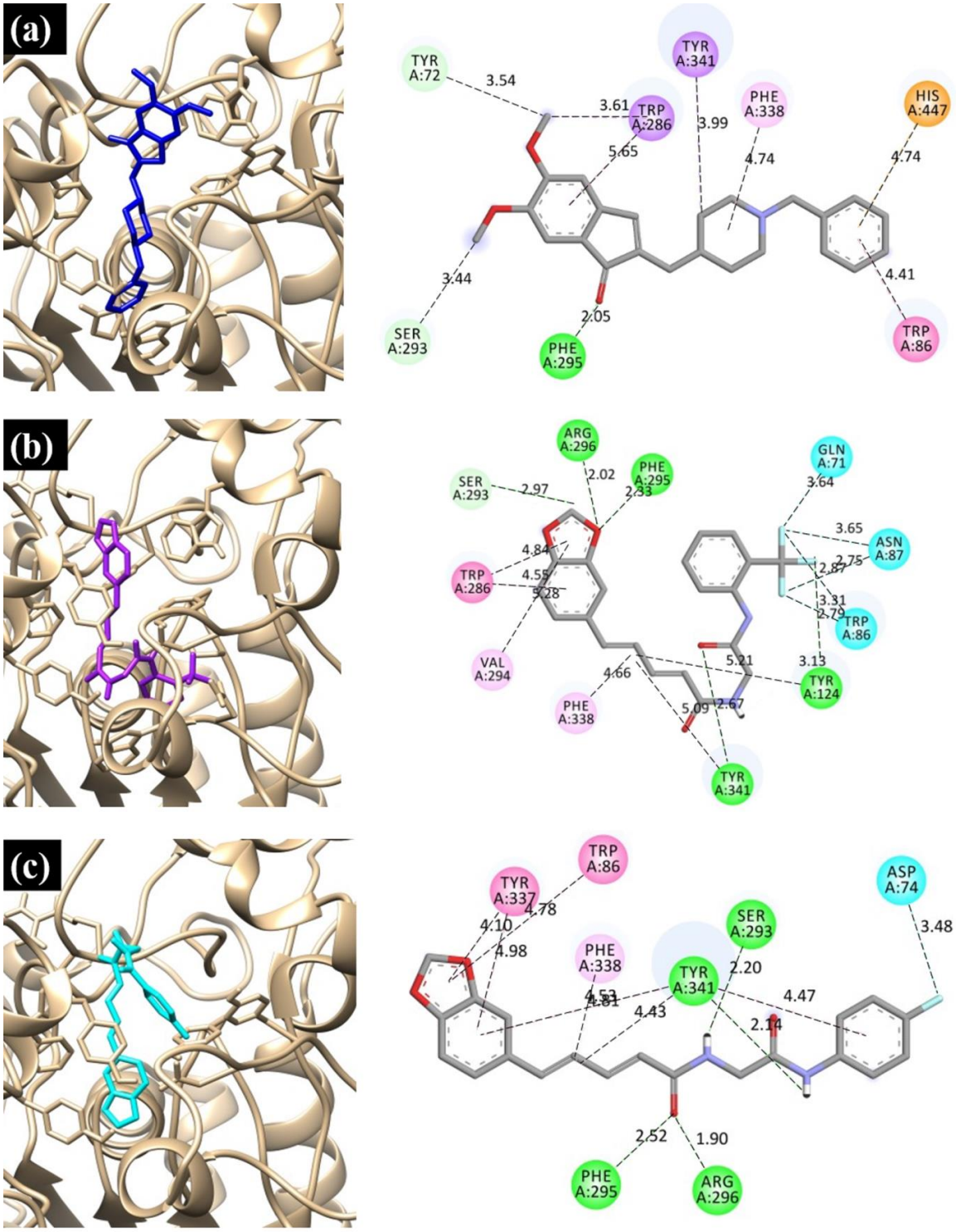

Figure. 4.4. Molecular interaction analysis (left: 3D binding poses and right: 2D interaction map) between the potent compounds and AChE protein (a) **DPZ**, (b) **6e** and (c) **6j**

4.2.6.2. Drug-likeness and ADMET prediction

To find out the drug-likeness properties of the compounds, physiochemical parameters were predicted using PaDEL-Descriptors (21). A Compound that does not qualify the

drug-likeness barriers often fails to meet the required criteria for becoming a potent clinical candidate. Generally, the compound needs to qualify all the criteria of Lipinski's Rule of Five (i.e., molecular weight < 500 g/mol, hydrogen bond acceptors < 10, hydrogen bond donor < 5, and LogP< 5) to be considered as a drug-like molecule. It was found that both **6e** and **6j** compounds obey Lipinski's Rule of Five with zero violations, suggesting their good bioavailability **(Table 1.4)**.

Table 1.4. Physiochemical parameters of the potent compounds predicted using Swiss ADME tool

Parameters	**DPZ**	**6e**	**6j**
Molecular weight (g/mol)	379.49	418.37	368.36
H-bond acceptors	4	7	5
H-bond donors	0	2	2
LogP	3.06	2.63	2.19
Lipinski rule violations	0	0	0
Solubility	Moderately soluble	Moderately soluble	Soluble

4.2.6.3. Molecular dynamic (MD) simulation Study

To get a deeper insight into the complex formation between the AChE protein and compound and to check their thermodynamic stability, MD simulations were carried out using the GROMACS simulation package 2020.3 (22). The best-docked pose of the compounds **6e** and **6j**, along with the reference compound DPZ, was simulated for 50 ns. The stability of the AChE upon compound binding was evaluated by r.m.s. deviations (RMSD), r.m.s. fluctuations (RMSF), hydrogen bond formations and radius of gyration (Rg). The RMSD oscillations were found to be stable for all compounds after 5 ns of simulation when compared to control protein with average RMSD of 0.25 (**DPZ**), 0.26 (**6e**) and 0.22 (**6j**) nm (**Fig. 4.5a**). The compounds **6e** and **6j** showed better stability than **DPZ** as relatively lesser fluctuations were noticed during the simulation period. The

RMSF fluctuations also corroborated the RMSD results with an average RMSF value of 0.15 (control protein), 0.15 (**DPZ**), 0.15 (**6e**) and 0.13 (**6j**) nm (**Fig. 4.5b**). This infers about the stability of the backbone of the protein upon binding with the compounds. The hydrogen bond forming capacity of the compounds is evident from the **Fig. 4.5c,** where a higher number of hydrogen bond formation was observed in the case of **6e** and **6j** compounds. The compactness of the complex was confirmed by Rg plot which showed better and similar compactness of the compounds compared to protein (**Fig. 4.5d**). These studies establish that the compounds **6e** and **6j** form stable complex with the AChE protein and have a potential to inhibit of the protein.

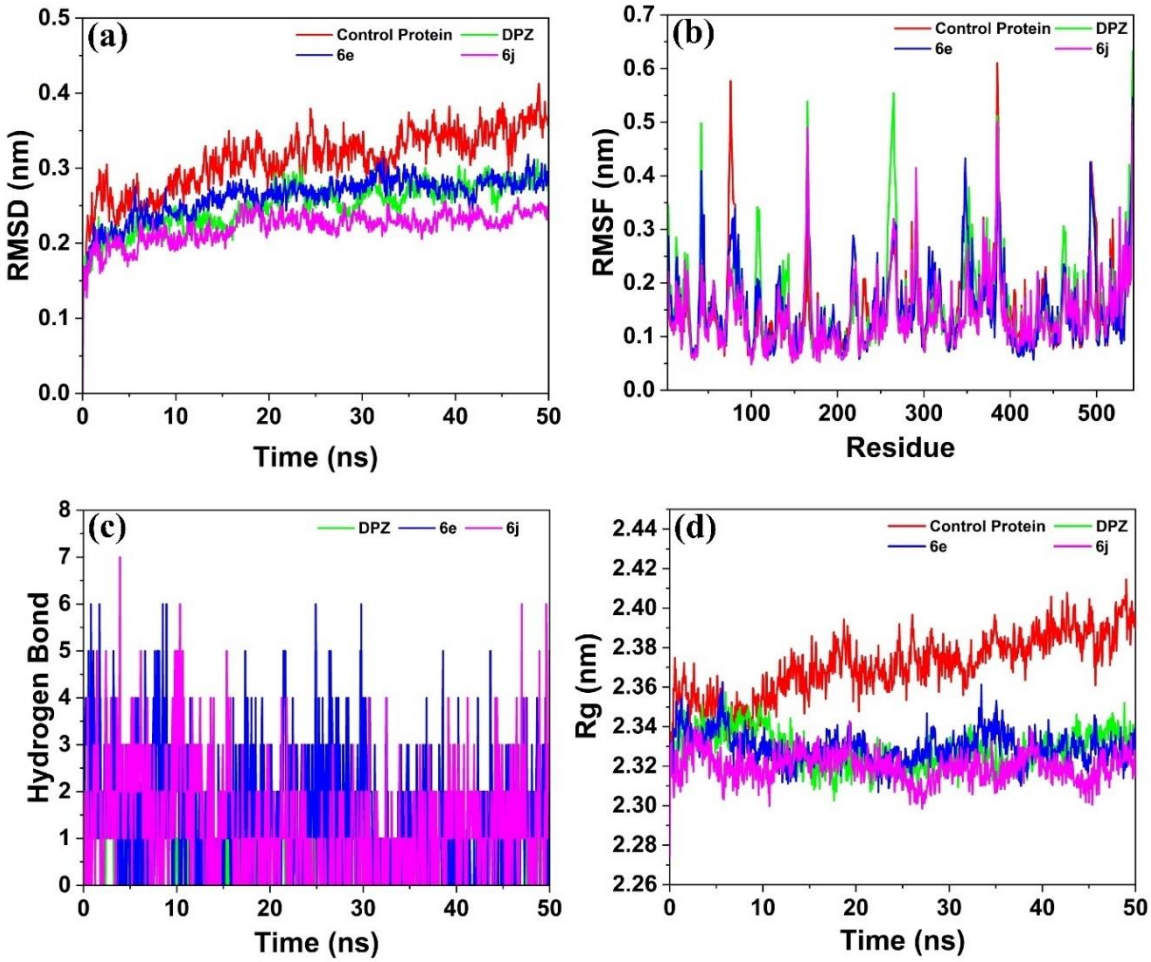

Figure. 4.5. Comparison of molecular dynamic simulation analysis of the potent compounds with AChE protein during a 50 ns simulation period; (a) RMSD, (b) RMSF, (c) hydrogen bond formation and (d) Rg plot.

4.2.6.4. Binding free energy calculations

To find out the free energy difference between the bound and completely unbound state of the compound and the protein, molecular mechanics-generalized born surface area (MM-GBSA) approach was utilized (23). The calculations were performed in GROMACS using *g-mmpbsa* module. Both the compounds **6e** (-207.87 kcal/mol) and **6j** (-211.943 kcal/mol) showed slightly lower negative energies compared to **DPZ** (-205.92 kcal/mol) which infers about their comparable binding affinities of the potent compounds.

4.2.6.5. Density functional theory (DFT) analysis of the potent compounds

To explore the atomic, electronic and energy states of the potent compounds, DFT analysis was carried out using the Gaussian 16W program (24). The output was evaluated as the total energy of the compound, HOMO (highest occupied molecular orbital) energy, LUMO (lowest unoccupied molecular orbital) energy, and band gap energy ($\Delta G = E_{LUMO} - E_{HOMO}$). The compounds showed a total electronic energy of -1519.525 kcal/mol (**6e**) and -1281.702 kcal/mol (**6j**), whereas, **DPZ** showed a lower negative value of -1212.132 kcal/mol which indicates the better binding of the compounds than **DPZ**. The stability of the potent compounds towards the protein was determined by band gap energy. Both the compounds **6e** (0.04 kcal/mol) and **6j** (0.04 kcal/mol) showed lesser band gap than **DPZ** (0.08 kcal/mol) (**Fig. 4.6**) suggesting their better chemical reactivity compared to **DPZ**. These results are in good agreement with the molecular docking and MD simulation results.

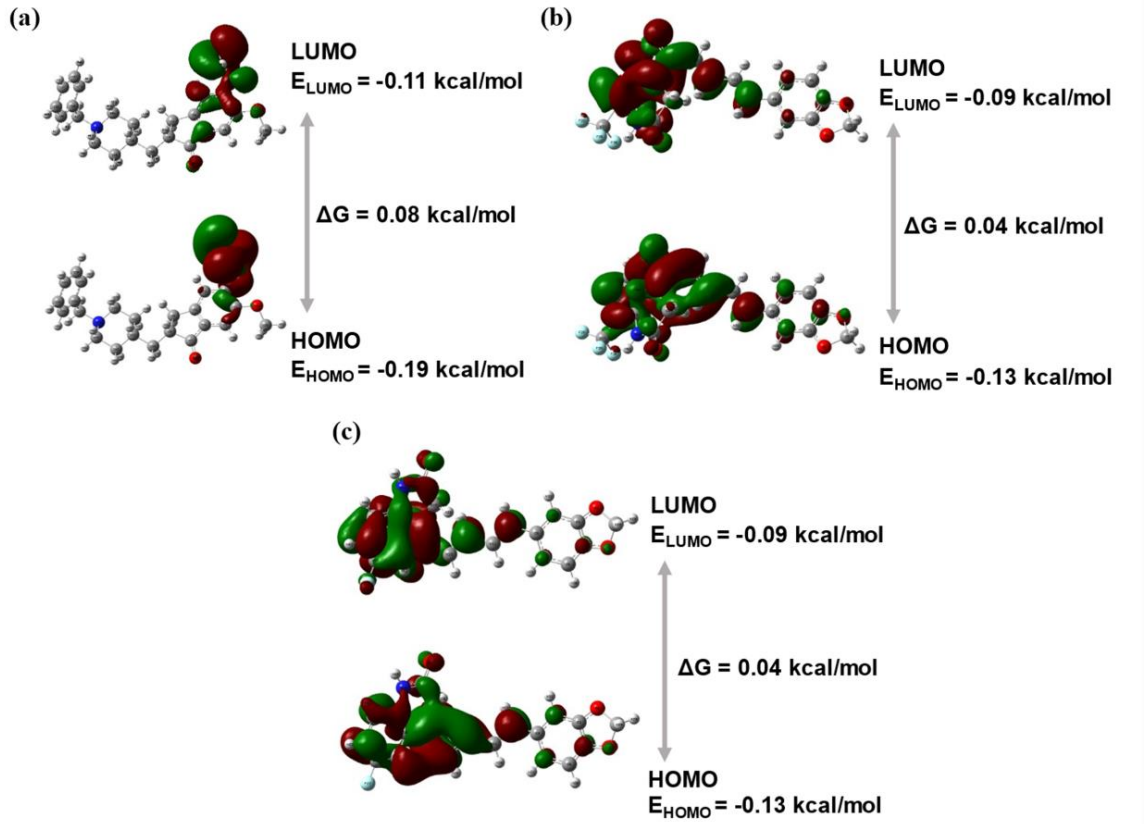

Figure. 4.6. Molecular orbitals of the compounds with HOMO, LUMO and band gap energy for the potent compounds (a) **DPZ**, (b) **6e** and (c) **6j**

The molecular electronic potential (MEP) maps also depicted the bond-forming capacity of the **6e** and **6j** compounds compared to **DPZ** based on the red electronegative region (H bond acceptor) and blue electropositive region (H bond donor) (**Fig. 4.7**). These results also support to the enhanced bond formation capacity of the potent compounds compared to **DPZ**.

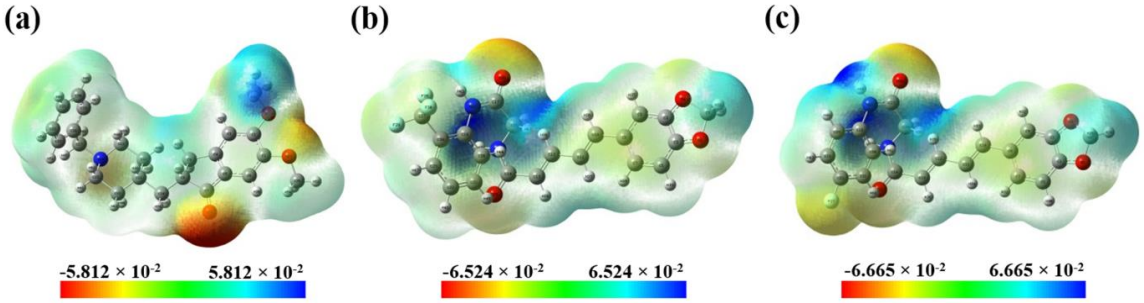

Figure. 4.7. The MEP maps for the compounds (a) **DPZ**, (b) **6e** and (c) **6j**

4.2.7. PAMPA assay for in-vitro analysis of permeability

The study described here aimed to measure the brain permeability of test compounds for developing anti-Alzheimer medication. The experiment used two generic drugs, testosterone and Norfloxacin, as standards for validation. Based on the results, compounds with a permeability value (Pe) greater than 4 had high BBB permeability, while those with a Pe value less than 2 had low BBB permeability. The analysis showed that test compound **6j** had a Pe value greater than 4, indicating that it could potentially cross the brain to reach its target (16). The permeability (Pe) of **6j**, testosterone, and Norfloxacin was determined in the PAMPA assay were expressed in Pe = 10^{-6} cm s^{-1}.

Table 1.5. Permeability (Pe) of **6j**, testosterone, and Norfloxacin in the PAMPA assay

S.No.	Compound	P_e (exp)[a]	Reference value[b]	Prediction[c]
1	6j	7.98	-------	CNS (+)
2.	Testosterone	18.43	17.0	CNS (+)
3.	Norfloxacin	0.12	0.1	CNS (-)

[b] Standard values of Norfloxacin and Testosterone were taken from literature given by Di Li et al.

4.2.8. Cytotoxicity study

The MTT assay is used to evaluate the cytotoxicity of a lead molecule (**6j**) by using different concentrations. The assay measures the reduction of MTT to formazan purple, which is a measure of cell viability(30, 32) Healthy and fast-growing cells reduce more MTT, resulting in higher absorbance, while dead or inactive cells do not show this activity. The MTT performed was used to observe the dose-dependent activity of **6j** on the SH-SY5Y cell line, a commonly used neuroblastoma cell line. Results showed in Figure 4.8 suggest that the treated cells were compatible with **6j** at all tested concentrations.

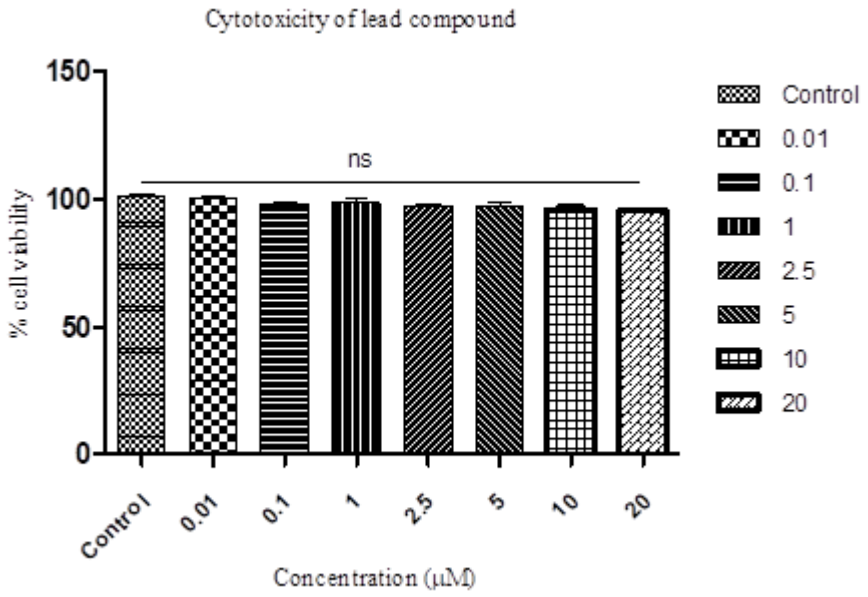

Figure. 4.8. The effect of **6j**, a lead molecule, on the viability of SH-SY5Y cells using the MTT assay. Cells were exposed to various concentrations (0.01, 0.1, 1, 2.5, 5, 10, and 20 µM) of a compound **6j** for a duration of 24 hours. The percent viability of SH-SY5Y cells was calculated as the mean ± SE from three separate experiments, each performed in triplicate

4.2.9. Acute toxicity studies in animals

Toxicity in the liver and kidneys is a critical factor in the development of a new drug, as these organs play a vital role in the metabolism and elimination of drugs and other chemicals from the body. The *in-vivo* acute toxicity study of **6j** was performed in male Swiss albino mice according to OECD guidelines. The lead compound was selected for the study due to its enzyme- inhibitory and multifunctional properties. Behavioral toxicity symptoms were observed starting from 4 hours after administration, and no alterations were observed in regards to water and food intake or weight reduction (**Fig. 4.9**). No animal deaths were recorded during the 14-day after the administration of **6j** up to a dose of 500 mg/kg (14). Further, the histopathological sections of kidney and liver (Fig. 1, SI, page # 48) which also did not shown any sign of toxicity.

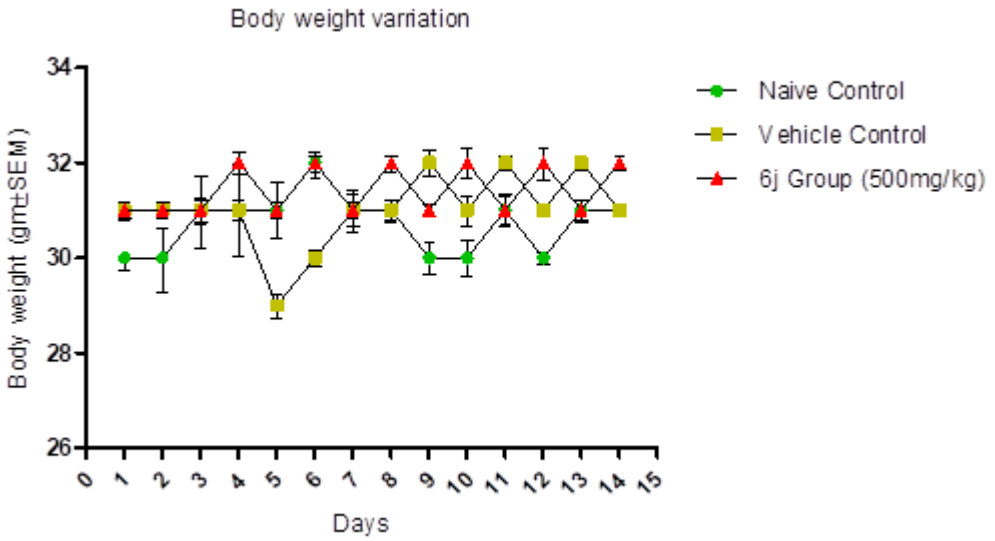

Figure. 4.9. Graphical representation of body weight of each group of mice up to 14th day of drug administration of**6j**, 500 mg/kg.

4.2.10. Y- Maze experiment for scopolamine-induced impairment on spatial memory

Y maze was performed to study the effectiveness of compound **6j** in improving learning and memory in mice suffering from dysfunctions. The mice were treated with a dose of either 5 mg/kg or 10 mg/kg of the compound daily for 7 days. The test was conducted on healthy mice (Swiss albino), and the mice's body weights were recorded during the experiment. The learning and memory impairments in the mice were induced using scopolamine, which blocks the muscarinic cholinergic receptors, a commonly used animal model for Alzheimer's disease(33, 34) .

The spatial working memory of mice was evaluated through the Y maze experiment on the 7th day after administering an intra-peritoneal dose of scopolamine hydrochloride (3.0 mg/kg). The animals received **6j or PA or DPZ** 30 minutes before scopolamine. The % spontaneous alternation in the group treated with scopolamine (3 mg/kg, i.p.) demonstrated a substantial decrease in comparison to the group that served as a vehicle control (**Fig. 12**, ***p 0.005). In contrast, the group treated with DPZ (5.0 mg/kg, p.o.) demonstrated a notably higher level of spontaneous alternation in comparison with the

scopolamine-treated group (###p 0.005). Interesting, the animal tread with **6j** were comparable, with statistically significant differences observed in the percentage of spontaneous alternation compared to the groups treated with scopolamine and DPZ **Fig. 4.10**). At the dose of 5 mg/kg and 10 mg/kg doses of **6j** found effective ($p < 0.001$) reverse spontoons alteration when compared to scopolamine, with a moderate significance ($p \leq 0.01$) when compared to DPZ. However, the administration of **PA** at doses of 10 mg/kg did not show any promising activity when compared to **6j** in terms of spontaneous alternation. The mechanism behind spontaneous alternation in the scopolamine model is believed to be caused by the anti-acetylcholinesterase properties of lead molecule **6j**, which effectively crosses the brain and acts as a potent cholinesterase inhibitor. The results, as shown in **Fig. 4.11**, indicate that the number of arm entries was consistent across all treatment groups, suggesting that scopolamine does not affect the mice's locomotor activity.

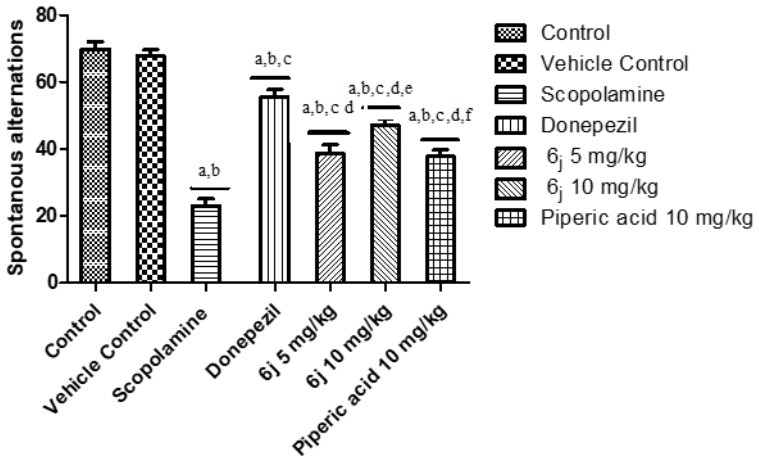

Figure. 4.10. The effect of Piperic acid (10 mg/kg), and its derivatives **6j** (5 & 10 mg/kg) on scopolamine induced – memory deficits in mice. Results are reported as mean ± standard deviation (SD) and are based on data collected from 6 mice. Data were analysed for statistical significance *via* one-way ANOVA following Newman-Keuls Multiple Comparison t-test, compared to control $^{a}p \leq 0.005$, ^{b} compared to vehicle control $^{b}p \leq 0.005$, compared to scopolamine $^{c}p \leq 0.005$, compared to Donepezil $^{d}p \leq 0.005$, compared to **6j** 5mg/kg, $^{e}p \leq 0.005$, compared to **6j** 10mg/kg, $^{f}p \leq 0.005$, compared to Piperic acid 10 mg/kg, $^{g}p \leq 0.005$

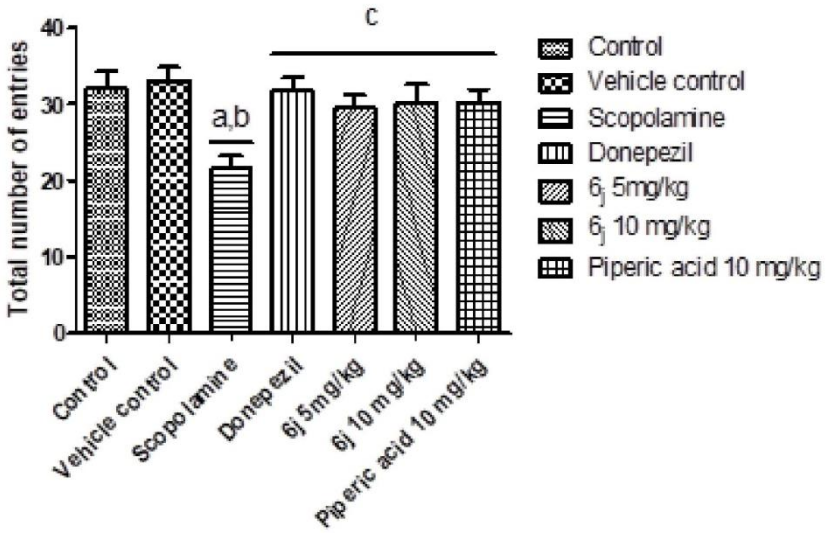

Figure 4.11. The effect of Piperic acid (10 mg/kg), and its derivatives **6j** (5 & 10 mg/kg) on scopolamine induced – memory deficits in mice. Results are reported as mean ± standard deviation (SD) and are based on data collected from 6 mice. Data were analysed for statistical significance *via* one-way ANOVA following Newman-Keuls Multiple Comparison t-test, compared to control $^{a}p \leq 0.005$, compared to vehicle control $^{b}p \leq 0.005$, compared to scopolamine $^{c}p \leq 0.005$

4.3.1. Chemistry of the second series of compounds

The synthesis of a novel series of piperic acid-benzyl piperazine derivatives **9a-9n** was carried out according to **scheme 1**. Commercially available benzyl halides (**7a-7m**) underwent nucleophilic substitution reaction (SN_2) with piperazine in ethanol to give compounds **8a-8m.** Final derivatives **9a-9m** were synthesized by the reaction of substituted benzylpiperazine (**8a-8m**) with **piperic acid** using the acid amide coupling in the presence of EDCI.HCl, hydroxybenzotriazole (HOBt), and triethylamine. Synthesized derivatives were purified by column chromatographic and characterization of synthesized derivatives by ^{1}H-NMR, ^{13}CNMR, and HRMS.(Singh et al., 2021)

Scheme 3. Synthesis of compounds **9a-9m**

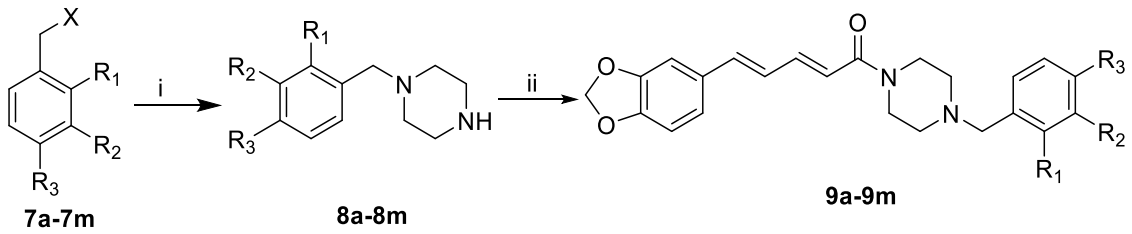

a: R_1 = H, R_2 = H, R_3 = H,
b: R_1 = CH_3, R_2 = H, R_3 = H
c: R_1 = H, R_2 = CH_3, R_3 = H,
d: R_1 = H, R_2 = H, R_3 = CH_3
e: R_1 = H, R_2 = H, R_3 = $(CH_3)_3CH$,
f: R_1 = F, R_2 = H, R_3 = H,
g: R_1 = H, R_2 = F, R_3 = H,
h: R_1 = H, R_2 =H, R_3 = F,
i: R_1 = H, R_2 = Cl, R_3 = H,
j: R_1 = H, R_2 = H, R_3 = Cl
k: R_1 = H, R_2 = NO_2 , R_3 = H,
l: R_1 = CN, R_2 = H, R_3 = F,
m: R_1 = H, R_2 = CN, R_3 = H,

Scheme 1. Synthesis of compounds **9a-9m**. Reagents and conditions: (i) Anhydrous piperazine, K_2CO_3, ethanol, reflux, 4-5 h, 70-80%; (ii) **PA**, EDCI.HCl, HOBT, DIPEA, dry THF, rt, overnight, 70-80%.

4.3.2. Biological evaluation of the second series of compounds

4.3.2.1. Cholinesterase inhibition studies

Considering the important role of ACh and BCh in memory and cognitive function, particularly in relation to AD, the inhibitory effect of the newly synthesized compounds on *h*AChE and *eq*BChE) was assessed using the spectroscopic method developed by Ellman and colleagues. To investigate the impact of structural modifications on enzyme inhibition properties, compound **9a** was synthesized and subsequently assessed for its inhibitory activity against cholinesterase (ChEs). During the enzyme inhibition studies, **9a**, which contained an unsubstituted benzylpiperazine fragment, demonstrated significant inhibitory activity against AChE. The % inhibition of **9a** against AChE was found to be 44.27 ± 0.07% and for BChE, 33.04 ± 2.54. To explore the impact of positional modifications on the phenyl ring of the benzylpiperazine fragment, methyl groups were introduced at different positions, resulting in the synthesis of compounds **9b-9d**. Intriguingly, the compounds with methyl groups positioned at various locations on the benzylpiperazine fragment exhibited similar inhibitory activity against AChE and

BChE, compared to compound **9a**. The IC_{50} values for compounds **9b-9d** against AChE and BChE were greater than 20 µM, indicating weak inhibition. The % inhibition for compounds **9b, 9c,** and **9d** against BChE were found to be 33.4 ± 1.67, 18.89 ± 2.64, and 2.26 ± 0.02 µM, respectively. These findings indicates that 3b-3d, demonstrated significant inhibitory effects on BChE over. This suggests that the structural modification involving the substitution of a methyl group on the benzylpiperazine scaffold resulted in improved inhibitory activity against BChE. We further introduced bulkier electron-donating groups (-*tert*-butyl) on the phenyl ring, to generate **9e** with equipotent activity against AChE and BChE compared to methyl substitution (**9b-9d**). Following the optimization of electron-donating groups, we proceeded to incorporate different electron-withdrawing groups (EWG) onto the phenyl ring. This allowed us to investigate the impact of substituents such as *o*-F, *m*-F, *p*-F, *m*-Cl, *p*-Cl, *m*-NO_2, *o*-CN and *m*-CN, *p*-CN. As a result, compounds **9f-9n** were synthesized. During the study on enzyme inhibition, it was observed that compounds **9m** and **9k**, harboring *m*-CN and *m*-NO_2 substituents on the phenyl ring, **9m** exhibited the highest level of inhibition against AChE compared to other analogs (AChE (μM), 4.26 ± 0.13) and **9k**, IC_{50} = 36.78 ± 2.02% respectively; **9m, 9k** BChE IC_{50} (μM), 1.03 ± 0.011 and % inhibition 54.94 ± 0.94 respectively. Compound **9n** bearing para-cyano group exhibited moderate AChE and BChE (46.06 ± 1.73% and 48.94 ± 0.33%, respectively) inhibition. In this study, a structure-activity relationship (SAR) was established by investigating different substitutions on the phenyl ring (as shown in Figure 2). Among the synthesized molecules, compound **9m**, which contained a small electron-withdrawing group, exhibited the highest potency against both AChE and BChE.

Table 1.6. AChE and equine BChE inhibition studies

Compound	R	*h*AChE % inhibition / IC_{50}[a] (μM)	*eq*BChE % inhibition / IC_{50} (μM)
9a	Hydrogen	44.27 ± 0.07 %	33.04 ± 2.54 %
9b	2-methyl	46.08 ± 0.46 %	33.4 ± 1.67 %
9c	3-methyl	44.81 ± 0.92 %	18.89 ± 2.64 %
9d	4-methyl	25.3 ± 0.44 %	2.26 ± 0.02 %
9e	*t*ert-butyl	42.71 ± 0.54 %	19.41 ± 1.17 %
9f	2-fluoro	42.12 ± 0.63 %	23.16 ± 1.88 %
9g	3-fluoro	44.30 ± 1.08 %	17.24 ± 0.99 %
9h	4-fluoro	43.36 ± 0.01 %	14.90 ± 1.09 %
9i	3-chloro	47.65 ± 0.97 %	37.87 ± 1.43 %
9j	4-chloro	48.96 ± 0.29 %	39.34 ± 1.09 %
9k	3-nitro	36.78 ± 2.02 %	54.94 ± 0.94 %
9l	2-cyano	25.59 ± 3.02 %	56.86 ± 1.41 %
9m	3-cyano	4.26 ± 0.13 μM	1.03 ± 0.011 μM
9n	4-cyano	46.06 ± 1.73 %	48.94 ± 0.33 %
PA	----	7.14 ± 0.98 %	5.87 ± 0.76 %
DPZ	----	0.06 ± 0.01 μM	2.16 ± 0.19 μM

[a]IC_{50}: measure of the 50 % effectiveness of a drug inhibition concentration (mean ± SD of two different assays).

[b]%: effectiveness of a drug inhibition at 20 μM of inhibitor

[d]**PA**(piperic acid) as parent molecule

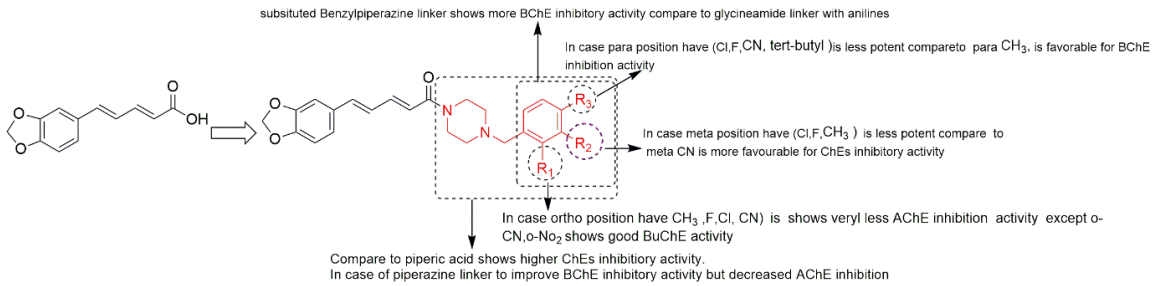

Figure. 4.12. Structural activity relationship of PA derivatives

4.3.2.2. Kinetic analysis of 9m on Cholinesterase's inhibition

The mechanism of inhibition of cholinesterase by **9m** was investigated using *h*AChE and*eq*BChE as the target enzyme was examined by conducting a study that involved plotting the reciprocal of the velocity [1/V] against reciprocal of the substrate [1/S] concentrations. The assay was carried out using different concentrations of **9m** (0.1,0.5 and 1 µM for BChE and 1,5,10 µM for AChE) in combination with five varying substrate concentrations (0.5, 1.0, 1.5, 2.0, and 2.5 µM). The results, depicted in Figure 4.13, indicated that compound 9m exhibited mixed inhibition in the case of hAChE and competitive inhibition in the case of eqBChE, as demonstrated by the Lineweaver-Burk reciprocal plots.

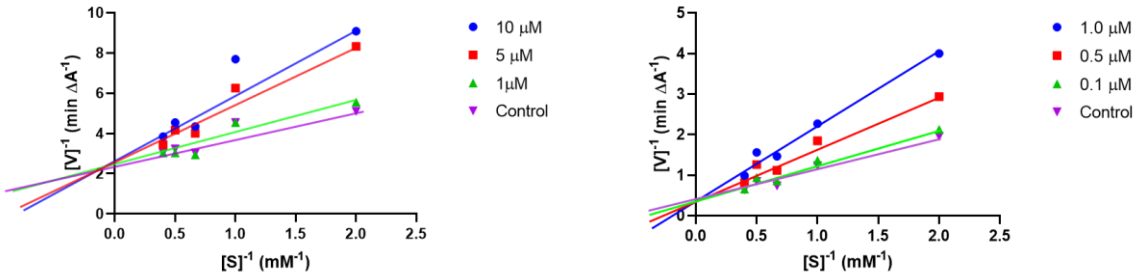

Figure. 4.13. Graphical representation of Lineweaver reciprocal plot depicting *h*AChE and *eq*BChE inhibition over a different substrate concentration; [**A**] *h*AChE inhibition by **9m** [**B**] *eq*BChE inhibition by **9m.**

4.3.2.3. Propidium iodide displacement assay

To assess the binding affinity of a newly synthesized molecule towards the peripheral anionic site (PAS) of human acetylcholinesterase (*h*AChE), an experiment was conducted using propidium iodide as a PAS-specific ligand. During the experiment, a decrease in the fluorescence intensity of propidium iodide was observed, indicating that the lead compound **9m** displaced propidium from the peripheral anionic site (PAS) of *h*AChE. The results displayed in Table 1.7 demonstrated that the test molecule **9m** exhibited a higher capability to displace propidium iodide, with a displacement percentage of 10.43

% at 50 µM, compared to the reference compound **PA**, which showed a displacement percentage of 4.99 % at 50 µM. Furthermore, the compound DPZ displayed a noteworthy displacement of 28.76 % at 50 µM, indicating a significant binding affinity towards the peripheral anionic site (PAS) of *h*AChE.

Table 1.7. Inhibition of the PAS by compound 3m

Compound	5 μM (%)	10 μM (%)	20 μM (%)	50 μM (%)
9m	1.03 ± 0.03	3.22 ± 0.24	5.89 ± 0.26	10.43 ± 0.56
PA	0.76± 0.21	1.79 ± 0.23	3.03 ± 0.08	4.99 ± 0.03
DPZ	9.56 ± 0.18	13.01 ± 0.35	19.71 ± 0.08	28.76 ± 0.39

[a]The results show the average value ± standard error of the mean, obtained from two independent experiments performed with three replicates each. DPZ = Donepezil

4.3.2.3. Evaluation of antioxidant activity by DPPH assay and metal chelation property

The available literature emphasizes the critical role of oxidative stress (OS) in the progression of Alzheimer's disease (AD). Consequently, a more effective approach for AD treatment would involve the simultaneous inhibition of cholinesterase (ChEs) and the reduction of oxidative stress. (Praticò, 2008)The DPPH radical is a stable free radical containing nitrogen and an unpaired electron. Different concentrations of 9m, 3k, 3g, and PA were subjected to antioxidant property evaluation in a standard DPPH assay. Due to the absence of an antioxidant component in the lead compounds, it is expected that the resulting hybrids would not exhibit any antioxidant activity at a concentration of 20 µM.

Studies have shown that imbalances in the levels of bimetals, such as iron and copper, in the brain may contribute to the development of AD. We conducted a study to understand the interaction of **9m** with $FeCl_3$, We used a UV spectrophotometer to measure the absorbance of **9m** alone and **9m** + $FeCl_3$ over a wavelength range of 400-650 nm. Based on the observations depicted in Figure S1(in supporting information) it was inferred that **9m** (300 µM) upon incubation with 1 equivalent of $FeCl_3$, no increase in absorption

intensity or the appearance of any new peaks across the entire spectral range. This outcome indicates that the compound **9m** did not effectively form a complex with $FeCl_3$.

4.3.2.4. Molecular modelling studies

4.3.2.4.1. Molecular docking

We performed a molecular docking study using Auto dock software to gain a clear insight into the binding interaction of compounds 9k and 9m against the hBChE enzyme (Protein PDB ID # 4BDS). The compounds 9k and **9m** exhibited better BChE enzyme inhibition activity in in-vitro studies. Therefore, we selected these compounds to further validate their BChE enzyme activity using computational tools. Compound **9k** showed binding energy -9.78 kcal/mol and formed π-π stacking and π-alkyl, interactions with Trp82 and Ala328., compound **9l** showed binding energy -8.71 kcal/mol and formed π- π stacking, π-alkyl, π-sigma, and amide- π stacking interactions with Ile69, Met437, Ala328, and Trp82 respectively. Similarly, the compound 9m showed the -9.34kcal/mol binding energy and interacted with different amino acid residues such as Tyr332, His438, and Ala328via, forming π-alkyl and π-π stacking, alkyl interaction and Gly116, Gly117, and Gln71 showed conventional hydrogen bond. The findings of this study corroborate in-vitro studies finding. Among these, the compound 3m shows exhibited the most promising binding interaction. Therefore, we selected **9m** for the molecular dynamics study.

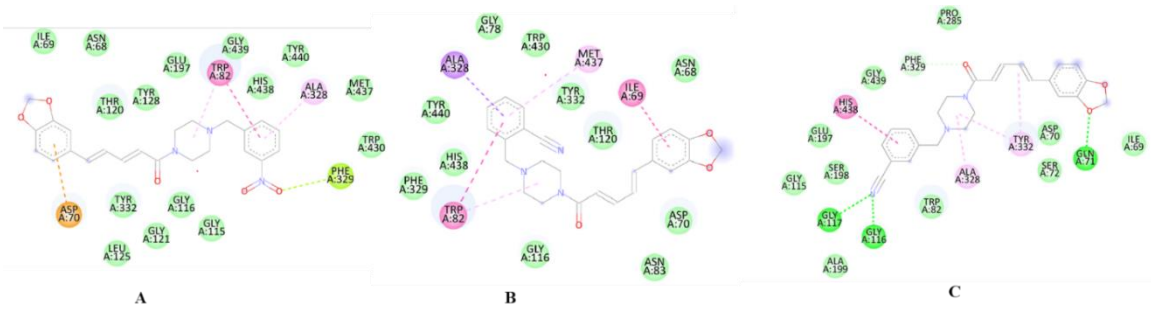

Figure. 4.14. A) The 2d interaction diagram of A, B, C is respectively **9k, 9l, and 9m** with BChE (Protein PDB ID: 4BDS)

4.3.2.4.2. Molecular dynamics

To gain a more comprehensive understanding of the complex formation between the BChE (PDB ID # 4bds) protein and compound **9m** and to assess their thermodynamic stability, an MD simulation study was conducted using the Gromacs 2020. The most favourable docked pose of compounds, **9m**, was subjected to a 100 ns simulation. The stability of the BChE protein upon binding with compound **9m** was evaluated through the analysis of several parameters, including root-mean-square deviations (RMSD) and root-mean-square fluctuations (RMSF). These measurements allowed for the assessment of how much the protein structure deviates from its initial conformation during the simulation and how flexible different regions of the protein are over the course of the simulation, respectively. These analyses provided valuable insights into the dynamic behaviour and thermodynamic stability of the BChE-compound complex. The protein (4BDS) bound to 9m exhibited an RMSD value in the range of 0.10 nm to 0.26 nm, which means the protein acquires a stable configuration throughout the simulation of 100 ns. At the same time, the ligand (9m) showed a RMSD value in the range of 0.29 nm to 0.90 nm. In the initial 40 ns of simulation, the compound experienced stable configuration and showed narrower fluctuation. After 40 ns and 60 ns, the compound experiences some conformational changes and shows more fluctuation, and then it acquires a stable configuration up to 100 ns. The RMSD result suggested that most of the time, ligand remains in the pocket of protein during the simulation. The protein RMSF was found in the range of 0.05 nm to 0.49 nm, whereas the ligand RMSF fell in the range of 0.04 nm to 0.26 nm, which suggested that the ligand showed less fluctuation and acquired a stable configuration. The RMSF data also corroborated the RMSD studies and did not show more flexibility in the protein backbone in forming a stable complex and providing stability to the compound **9m**.

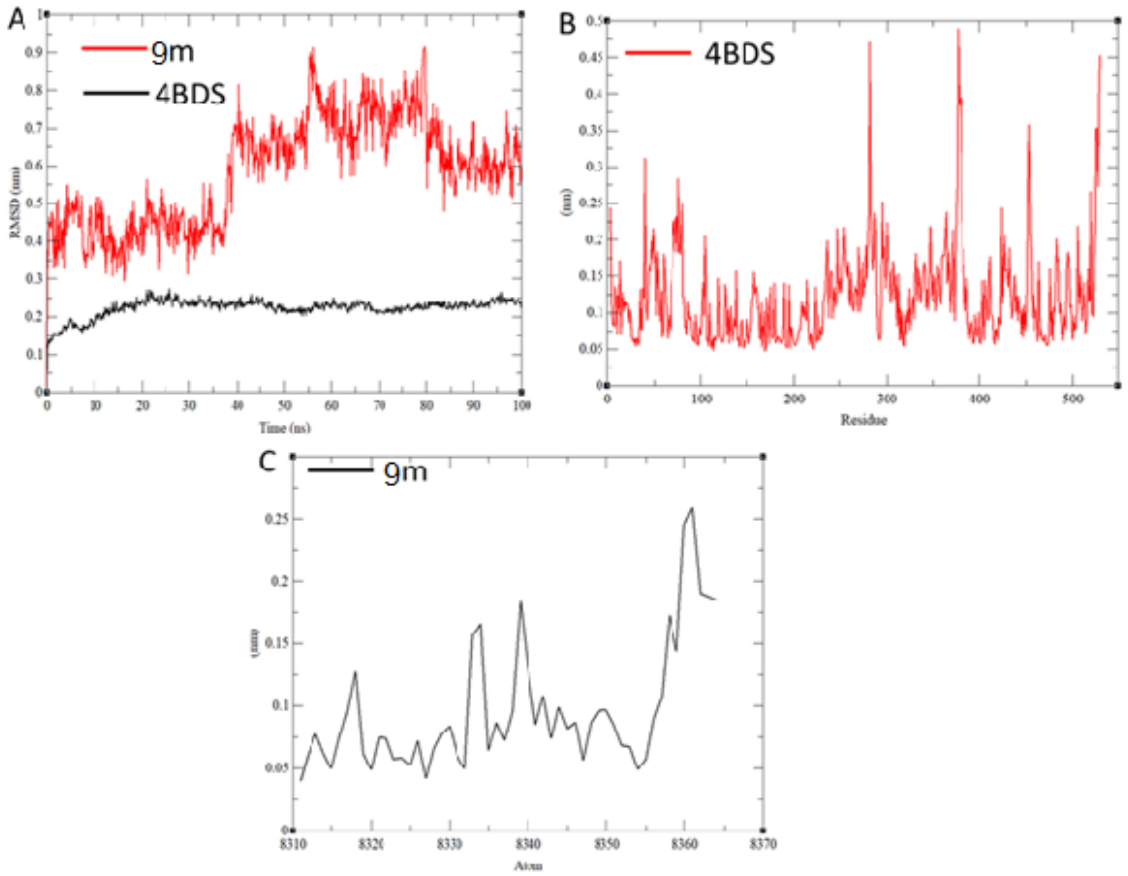

Figure. 4.15. The molecular dynamic studies for target compound **9m**. A) Root mean square (RMSD) deviation diagram of **9m**, B) Root mean fluctuation (RMSF) diagram of protein. C) Root mean fluctuation (RMSF) diagram of ligand.

4.3.2.4.3. Density functional theory (DFT) analysis of lead compound 3m:

The atomic, electronic, and energy states of the potent compounds were investigated through DFT analysis using the Gaussian 16W program. The analysis involved evaluating various parameters such as HOMO (highest occupied molecular orbital) energy, LUMO (lowest unoccupied molecular orbital) energy, and the band gap energy ($\Delta G = E_{LUMO} - E_{HOMO}$). The stability of the potent compound **9m** concerning protein binding was determined based on their band gap energy. The E_{LUMO} energy of the compound was found to be -2.204 eV whereas the E_{HOMO} of the compound was -5.802 eV. The band gap energy of compound 3m was observed (3m, ΔG = 3.59 eV). The compound **9m** showed lesser band gap energy, which means that the compound 9m possesses better chemical

reactivity. These finding corroborated with the findings of molecular docking and molecular dynamics findings of the compound **9m**.

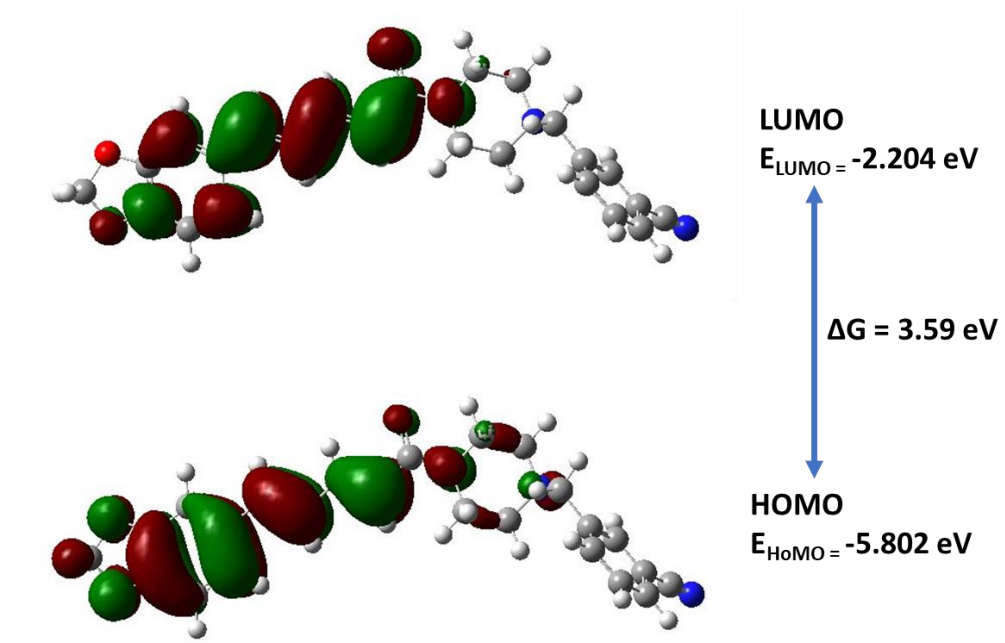

Figure. 4.16. The molecular orbitals of the compound, featuring the HOMO, LUMO, and band gap energy, are illustrated for the potent compound **9m**.

The molecular electrostatic potential (MEP) maps provided valuable insights into the bond-forming capabilities of compound **9m**. The maps displayed in red regions, indicating electronegative regions (H bond acceptors), and blue regions, representing electropositive regions (H bond donors) (as shown in Fig. 4.17).

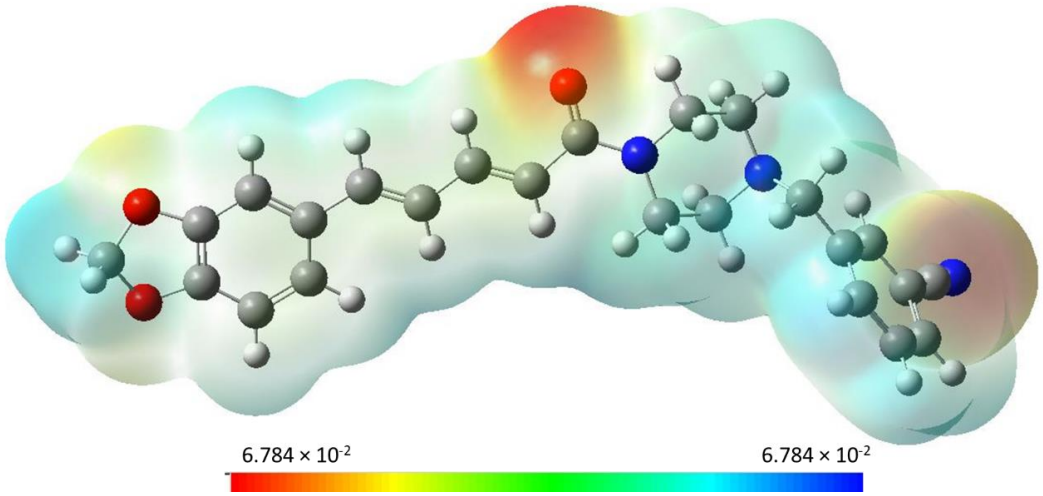

Figure. 4.17. The molecular electrostatic potential (MEP) maps for the compound **9m**.

The MEP maps further confirmed the enhanced bond formation capacity of the potent compound **9m**. These results provide additional support that **9m** have better bond forming abilities due to which it forms bond with different amino acid residues of target protein and shows the activity.

4.3.2.5. PAMPA assay to evaluate BBB permeability

The objective of this study was to assess the ability of test compounds to penetrate the brain and determine their potential for the development of medications targeting AD. As a means of validation, two reference drugs, corticosterone and hydrocortisone, were employed in the experiment. According to the findings, compounds that exhibits a permeability value (*Pe*) higher than 4 can be classified as a high permeability across the blood-brain barrier (BBB), whereas compounds with a *Pe* value lower than 2 were categorized as low BBB permeability. The analysis revealed that the test compound **9m** displayed a *Pe* value exceeding 4, indicating its potential ability to traverse the blood-brain barrier and reaching to its intended target within the brain.

Table 1.8. Permeability (Pe) of **9m**, testosterone, and Corticosterone in the PAMPA assay.

S.No.	Compound	P_e (exp)[a]	Reference value[b]	Prediction[c]
2.	Corticosterone	6.21 ± 1.03	5.1	CNS (+)
3.	Hydrocortisone	1.65 ± 0.56	1.9	CNS (-)
3.	**9m**	5.79 ± 1.12	-------	CNS (+)

Data are the mean ± SD of two independent experiments.

[a]Hydrocortisone were assessed using the PAMPA assay and were reported in units of Pe = 10^{-6} cm s^{-1}.(Di et al., 2003)

[b] Standard values of Corticosterone and Hydrocortisone were taken from literature given by Di Li et al.(Di et al., 2003),

4.3.2.6. Assessment of cytotoxicity of 9m in PC-12 cells

The MTT assay was performed to assess the cytotoxic effects of various concentrations of compound **9m** on PC12 cells. The assay quantifies the ability of nicotinamide adenine

dinucleotide phosphate (NADPH) -dependent cellular oxidoreductase enzymes to reduce MTT to the purple formazan crystals. Viable, metabolically active cells exhibit a greater reduction of MTT, leading to increased absorbance levels, which serves as an indicator of viability. PC-12 cell line, which is widely used as a neuronal study model after differentiation, was used for MTT assay. PC-12 cells were seeded at a concentration of 1 × 10^4 cells/well in 96 well plates and were incubated overnight for adherence. The compound (**9m**) was added at a concentration of 20, 15, 10, 7, 5, 2.5, 1, and 0.1 µM and incubated for 24h at 5% CO2 at 37°C. The MTT reagent (5mg/ml) was added and incubated for 3 h at 37°C, formazan crystals were dissolved by DMSO, and the reading was taken at 562 nm on Spectramax-i3x. The findings presented in Figure 4.18 indicate that the cytotoxicity of the compound in PC-12 cells treated with different concentrations of **9m**. It was observed that the compound (**9m**) showed no significant decrease in cell viability even when the concentration was increased up to 20 µM at which the cell viability was approximately 82.83%.

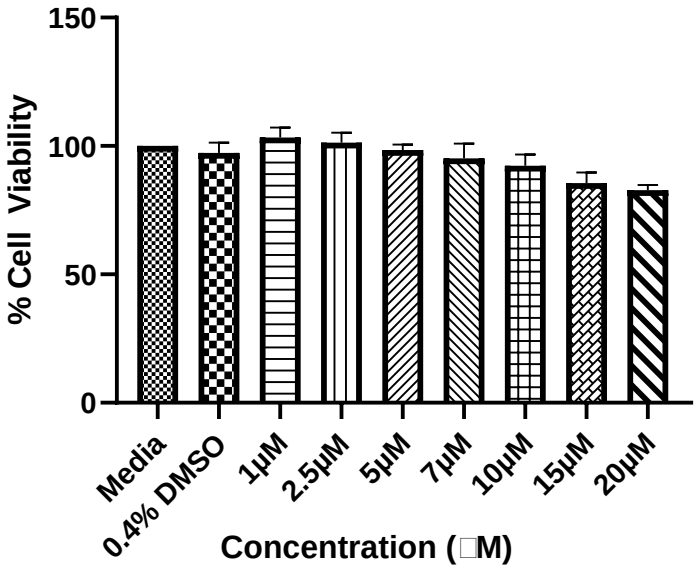

Figure. 4.18. The effect of **9m**, a lead molecule, on the viability of PC-12 cells using the MTT assay. Cells were exposed to various concentrations (1, 2.5, 5, 10, 15 and 20 µM) of a compound **9m** for a duration of 24 h. The percent viability of PC-12 cells is represented as the mean ± SE.

4.3.2.7. Effect of Compound 9m on H_2O_2 induced oxidative stress in PC12 cells:

Hydrogen peroxide (H_2O_2) is recognized as a significant producer of reactive oxygen species (ROS) and is believed to have a crucial involvement in the development of various chronic neurodegenerative disorders. Oxidative stress plays a crucial role in the initiation and progression of AD; effectively safeguarding neurons from oxidative damage could potentially have a significant impact on preventing disease advancement during the early stages of AD. This protective measure may also help to inhibit adverse consequences in AD pathology. Therefore, we have used H_2O_2-induced oxidative stress in the PC12 cell line as an in-vitro model of oxidative stress, which is used to assess the neuroprotective effect of **9m**.

Based on our earlier observation, we selected 600 µM of H_2O_2 to evaluate the potential of **9m** towards the oxidate stress-induced cell death. Differentiated PC-12 cells were grown in a 96-well plate and incubated with compound (**9m**) for 24 h at 20µM, 10µM, 7µM, 5µM, 2.5µM and 1µM concentrations, next cells were treated with 600 µM H_2O_2 which was used for inducing oxidative stress (SI, S2). The H2O2-treated group without compound showed only 55.5% cell viability. The compound (**9m**) showed a maximum of 71.17 % of cell viability at 10 µM (Figure 4.19B).

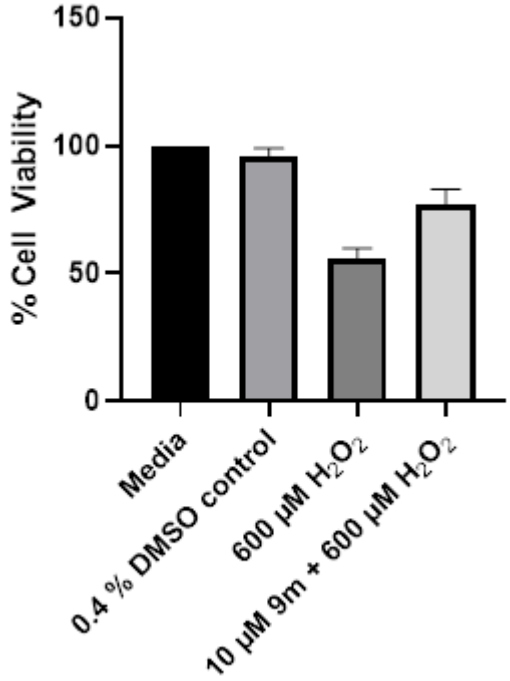

Figure. 4.19. Effect of **9m** against H_2O_2 mediated cell death. The data represents mean ± SEM.

4.3.2.8. Acute toxicity studies in animals

Assessing the potentially harmful effects is vital to ensure the safety and efficacy of the new molecules. Following the guidelines set by the OECD-425, an *in-vivo* acute toxicity study of compound **9m** was conducted on male Swiss albino mice. The selection of this lead compound for the study was based on its multifunctional properties and its ability to inhibit enzymes. Behavioral toxicity symptoms were observed in the mice starting 4 h after the administration of compound **9m**. However, there were no noticeable changes in water and food intake or any significant reduction in body weight, as shown in Figure 4.20. Importantly, there no fatalities recorded throughout the duration of the 14-day experiment. The experiment's findings indicated that the administration of drug **9m** to the animals did not exhibit any indications of liver or kidney toxicity even at a dosage of 500 mg/kg body weight over a period of 14 days.

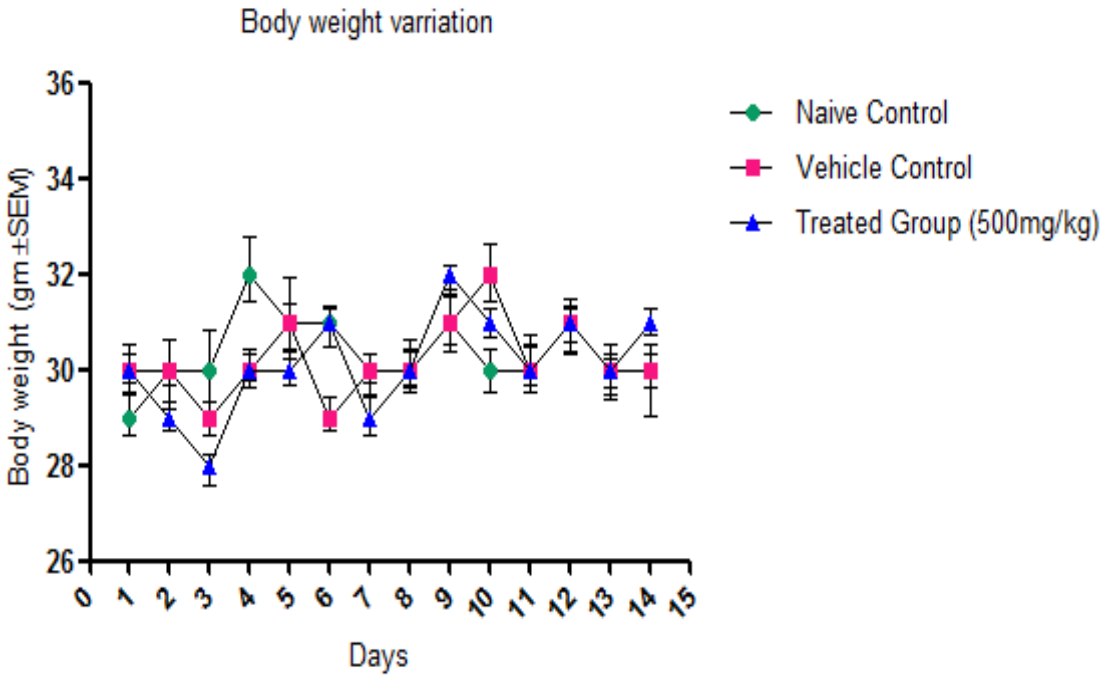

Figure. 4.20. Graphical representation of body weight of each group of mice up to 14th day of drug administration of **9m**, 500 mg/kg.

4.3.2.9. Evaluation of improvement of spatial memory in scopolamine-induced mice model

The Y-maze test was conducted to investigate the efficacy of compound **9m** in enhancing learning and memory in mice. The mice in the study were administered either a daily dose of 10 mg/kg or 20 mg/kg, *p.o.* of compound **9m** for a duration of 7 days. The experiment was performed on healthy Swiss albino mice, and the weights of the mice were monitored throughout the course of the study. To induce learning and memory impairments in the mice, scopolamine was utilized. Scopolamine acts by blocking the muscarinic cholinergic receptors and is a widely employed animal model for studying AD.

On the 7th day of the experiment, the spatial working memory of the mice was assessed using the Y-maze test. Prior to the evaluation, the mice were given an intra-peritoneal dose of scopolamine hydrochloride at a concentration of 3.0 mg/kg. The purpose of administering scopolamine was to induce spatial working memory impairments in the

mice for the subsequent evaluation. Prior to the administration of scopolamine, the animal was given **9m**/PA/DPZ, and this was done 30 min prior to the scopolamine treatment. In the group treated with scopolamine (3 mg/kg, i.p.), there was a significant decrease was observed in the percentage of spontaneous alternation compared to the group that received the vehicle control. This finding is depicted in Figure 4.21, and the statistical analysis revealed a significant difference with a p-value of less than 0.05 (***). Conversely, the group that received the positive control, DPZ (5.0 mg/kg, p.o.), exhibited a significantly higher level of spontaneous alternation when compared to the scopolamine-treated group. This notable difference is indicated in the results, with a statistically significant *p*-value of less than 0.05. The findings for compound **9m** were consistent, showing statistically significant variations in the percentage of spontaneous alternation compared to both the scopolamine-treated group and the DPZ-treated group (refer to Figure 4.21). The doses of **9m** at 10 mg/kg and 20 mg/kg demonstrated effectiveness with a high level of significance ($p < 0.05$) compared to the scopolamine group and a moderate level of significance ($p \leq 0.05$) compared to the DPZ group. In contrast, the administration of PA at doses of 20 mg/kg exhibits slight improvement in activity when compared to scopolamine in terms of spontaneous alternation. The results depicted in Figure 4.21 demonstrate that the number of arm entries remained consistent across all treatment groups, indicating that the administration of scopolamine did not impact the locomotor activity of the mice.

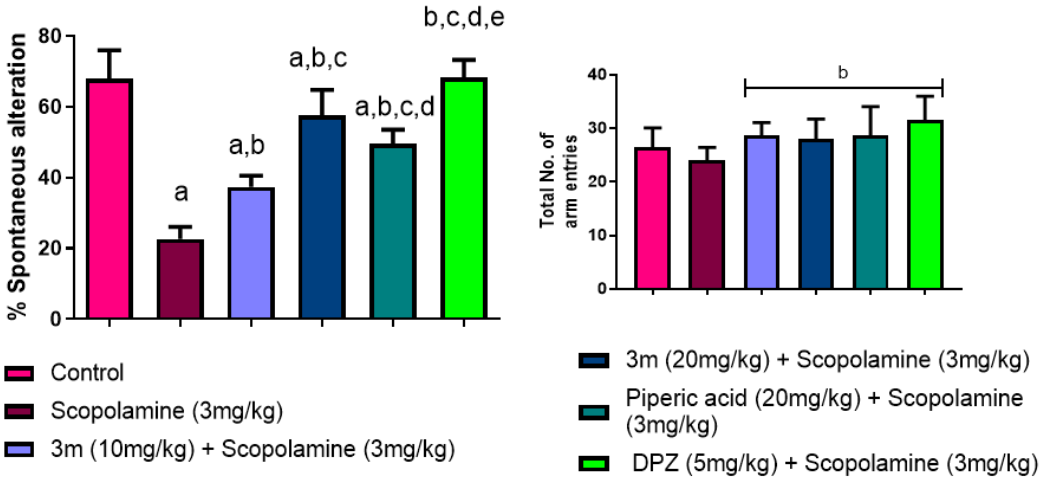

Figure. 4.21. The effect of donepezil (5mg/kg), Piperic acid (20 mg/kg), and its derivatives 9m (10mg/kg), 9m (20mg/kg) on scopolamine induced –memory deficits in mice. All values are in mean ± SD (n=6; number of mice). a $p \leq 0.05$ compared to control, b $p \leq 0.05$ compared to Scopolamine (3 mg/kg), c $p \leq 0.05$ compared to 9m (10mg/kg) + Scopolamine (3 mg/kg)) , d $p \leq 0.05$ compared to 9m (20mg/kg) + Scopolamine (3mg/kg), e $p \leq 0.05$ compared to Piperic acid (20mg/kg) + Scopolamine (3mg/kg), f $p \leq 0.05$ compared to DPZ (5 mg/kg) + Scopolamine (3 mg/kg), (one-way ANOVA followed by Newman-keuls Multiple Comparison t test).